Sources of Formaldehyde in U.S. Oil and Gas Production Regions

Dix, Barbara; Li, Meng; Roosenbrand, Esther; Francoeur, Colby; Brown, Steven S.; Gilman, Jessica B.; Hanisco, Thomas F.; Veefkind, J. Pepijn; Levelt, Pieternel F.; More Authors

DOI
10.1021/acsearthspacechem.3c00203

Publication date
2023

Document Version
Final published version

Published in
ACS Earth and Space Chemistry

ACS EARTH AND SPACE CHEMISTRY

http://pubs.acs.org/journal/aesccq

Article

Sources of Formaldehyde in U.S. Oil and Gas Production Regions

Barbara Dix,* Meng Li, Esther Roosenbrand, Colby Francoeur, Steven S. Brown, Jessica B. Gilman, Thomas F. Hanisco, Frank Keutsch, Abigail Koss, Brian M. Lerner, Jeff Peischl, James M. Roberts, Thomas B. Ryerson, Jason M. St. Clair, Patrick R. Veres, Carsten Warneke, Robert J. Wild, Glenn M. Wolfe, Bin Yuan, J. Pepijn Veefkind, Pieternel F. Levelt, Brian C. McDonald, and Joost de Gouw

Cite This: https://doi.org/10.1021/acsearthspacechem.3c00203

Read Online

ACCESS | Metrics & More | Article Recommendations | Supporting Information

ABSTRACT: We analyzed observational and model data to study the sources of formaldehyde over oil and gas production regions and to investigate how these observations may be used to constrain oil and gas volatile organic compound (VOC) emissions. The analysis of aircraft and satellite data consistently found that formaldehyde over oil and gas production regions during spring and summer is mostly formed by the photooxidation of precursor VOCs. Formaldehyde columns over the Permian Basin, one of the largest oil- and gas-producing regions in the United States, are correlated with the production locations. Formaldehyde simulations by the atmospheric chemistry and transport model WRF-Chem, which included oil and gas NO_x and VOC emissions from the fuel-based oil and gas inventory, were in very good agreement with TROPOMI satellite measurements. Sensitivity studies illustrated that VOCs released from oil and gas activities are important precursors to formaldehyde, but other sources of VOCs contribute as well and that the formation of secondary formaldehyde is highly sensitive to NO_x. We also investigated the ability of the chemical mechanism used in WRF-Chem to represent formaldehyde formation from oil and gas hydrocarbons by comparing against the Master Chemical Mechanism. Further, our work provides estimates of primary formaldehyde emissions from oil and gas production activities, with per basin averages ranging from 0.07 to 2.2 kg h^{-1} in 2018. A separate estimate for natural gas flaring found that flaring emissions could contribute 5 to 12% to the total primary formaldehyde emissions for the Permian Basin in 2018.

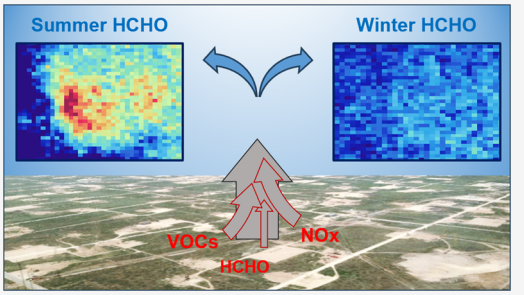

KEYWORDS: *formaldehyde, oil and gas, emissions, VOCs, NO_x, air quality*

1. INTRODUCTION

The production of crude oil and natural gas in the United States has seen rapid growth since the mid-2000s due to the development and use of horizontal drilling and hydraulic fracturing. The emissions of methane associated with this activity have received ample attention (e.g.,[1−4]). Also important are emissions of air pollutants such as nitrogen oxides (NO_x) and volatile organic compounds (VOCs), which can react to form ozone in the sunlit atmosphere.[5] The emissions of VOCs are poorly constrained.[3,6−8] For example, Pétron et al.[8] found that benzene emissions in the Denver-Julesburg Basin were significantly underestimated in different emission inventories, Ahmadov et al.[7] showed that VOC emissions in the Uintah Basin in Utah were underestimated by a factor of ∼2 in the regulatory emission inventory, and a study by Holliman and Schade[9] suggested that hydrocarbon emissions are in exceedance of permits in the Eagle Ford Shale in Texas.

Most production regions in the United States are in relatively remote regions, where ground-based pollution measurements are sparse or nonexistent. Satellite remote sensing data have therefore played an important role in quantifying the emissions of methane and nitrogen oxides.[2,10−14] Satellite measurements of the nonmethane hydrocarbons released from oil and gas are not available to date. What is available are measurements of formaldehyde (HCHO), which can be released as a combustion byproduct and formed in the atmosphere from the photooxidation of precursor VOCs. Satellite measurements of formaldehyde have been used to constrain biogenic emissions of isoprene, which is very efficient in forming formaldehyde.[15] The goal of this work is to study the sources of formaldehyde in oil and gas production regions with an eye toward using the measurements to constrain oil and gas VOC emissions. Questions we

Received: July 11, 2023
Revised: October 15, 2023
Accepted: October 23, 2023

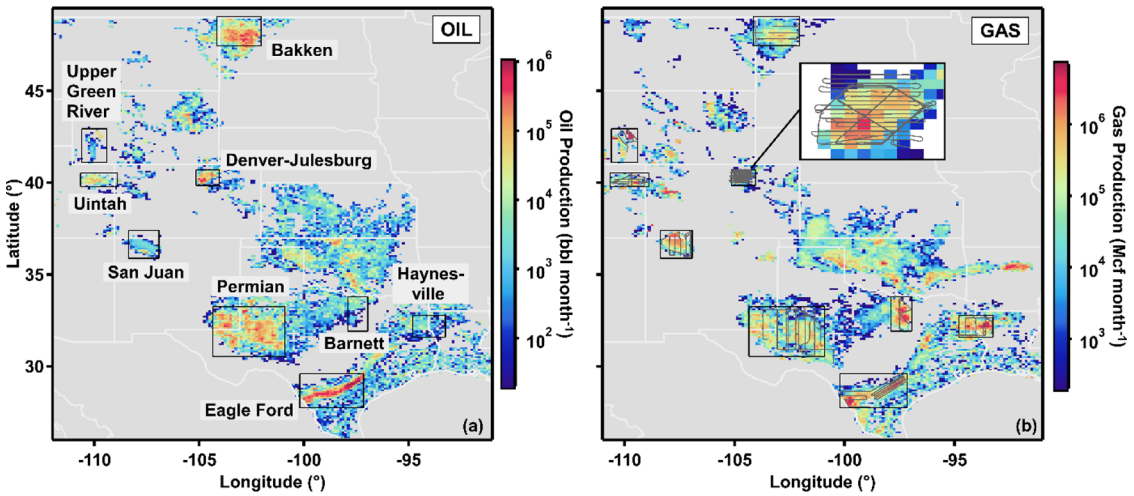

Figure 1. Oil and natural gas production regions sampled by the SONGNEX aircraft campaign shown on top of average oil (a) and gas (b) production volumes for March and April 2015 (Enverus DrillingInfo database; see Section 2.5). The black boxes outline the areas used for data analysis in this study, and flight tracks within these areas are included in panel (b), where the inset shows a zoom on the Denver-Julesburg Basin. The background maps are scaled in industry standard units: oil production in barrels (bbl) per month and natural gas production in 1000 cubic feet (Mcf) per month.

focused on include the relative contributions of direct emissions versus the chemical formation of formaldehyde and the importance of oil and gas hydrocarbons as formaldehyde precursors. Understanding VOC emissions from oil and gas production has important implications for understanding air quality and mitigating pollution. Not only do these emissions contribute to ground-level ozone pollution, but some of the oil- and gas-related VOCs are very harmful to human health, such as benzene and formaldehyde itself, which are listed by the U.S. Environmental Protection Agency as hazardous air pollutants.[16]

In this article, we will first analyze measurements of formaldehyde made during the 2015 NOAA Shale Oil and Natural Gas NEXus (SONGNEX) study. During SONGNEX, the NOAA WP-3D research aircraft was used to measure atmospheric composition in multiple oil and gas production regions in the central United States. Our analysis focuses on quantifying the relative importance of direct emissions and secondary formation of formaldehyde. Next, we describe the observed formaldehyde columns from the satellite-based TROPOspheric Monitoring Instrument (TROPOMI) over the Permian Basin in Texas, where oil and gas production is high. We compare the observed formaldehyde columns with output from the Weather Research and Forecasting coupled with Chemistry model (WRF-Chem) using our recently reported emission estimates of NO_x and VOCs from oil and gas production[3] and report results from several sensitivity runs with the model that tests the dependence of formaldehyde formation on emissions of oil and gas NO_x and VOCs. We also test the ability of the chemical mechanism used in the WRF-Chem model to accurately describe formaldehyde formation from oil and gas VOCs using zero-dimensional (0-D) model calculations with the Master Chemical Mechanism. Finally, we use our results to estimate direct emissions of formaldehyde from oil and gas operations in different basins in the United States and discuss how these estimates compare to observations.

2. DATA AND METHODS

2.1. SONGNEX Campaign. The NOAA Shale Oil and Natural Gas Nexus (SONGNEX) study was conducted in March and April 2015. For this mission, the NOAA WP-3D research aircraft was equipped with multiple instruments to quantify greenhouse gases and air pollutants from oil and gas production as well as the products formed in the atmosphere from the oxidation of these emissions. SONGNEX flights included sampling in the following oil and natural gas basins: Bakken in North Dakota, the Upper Green River in Wyoming, the Uintah Basin in Utah, the Denver-Julesburg Basin in Colorado, the San Juan Basin in New Mexico, and the Permian Basin, Eagle Ford, Barnett, and Haynesville regions in Texas. Outlines of the sampled regions and flight tracks are depicted in Figure 1 on top of the oil and natural gas production volumes during March and April 2015.

In this study, we use data from the following measurements:[17]

- Formaldehyde was measured by laser-induced fluorescence.[18]
- Nitrogen oxides and ozone were measured by cavity-ringdown spectroscopy.
- Acyl peroxy nitrates were measured by chemical ionization mass spectrometry.
- Methane was measured by IR laser absorption in a high-finesse cavity.[4]
- VOCs were measured in flight by proton-transfer-reaction time-of-flight mass spectrometry[19] and by postflight gas chromatography−mass spectrometry analysis of canister samples.[20]
- Sulfur dioxide was measured by pulsed ultraviolet fluorescence.
- Pressure, temperature, and relative humidity were measured by the NOAA WP-3D onboard instruments.[17]

For analysis, all flight data were filtered to include boundary layer legs only. Further, time periods with distinct and anomalous high spikes in SO_2 were used to remove data that likely contain emissions from large industrial sources, such as power plants.

https://doi.org/10.1021/acsearthspacechem.3c00203
ACS Earth Space Chem. XXXX, XXX, XXX−XXX

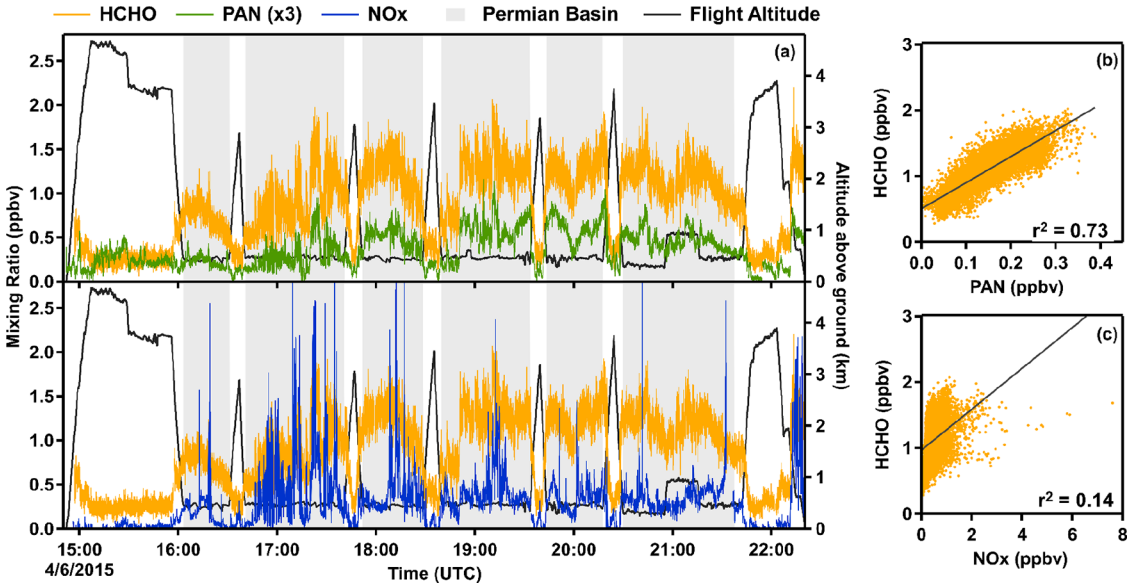

Figure 2. Analysis of formaldehyde data from the SONGNEX flight on 6 April 2015 over the Permian Basin. (a) Formaldehyde data with PAN (top) and formaldehyde together with NO_x (bottom). The gray-shaded areas denote the data obtained within the boundary layer that are used in subsequent analyses. Note that PAN here is scaled by a factor of 3. (b, c) Correlation between formaldehyde and PAN and NO_x, respectively. Line fits and the Pearson correlation coefficients r^2 are added and show the higher correlation between formaldehyde and PAN.

2.2. TROPOMI Satellite Data. The TROPOMI is a spectrometer on ESA's Copernicus Sentinel-5 Precursor satellite.[21] The instrument provides daily global coverage of formaldehyde, NO_2, and other trace gases with a spatial resolution at nadir of 3.5 × 5.5 km^2 (3.5 × 7.0 km^2 before 6 August 2019) for the UV−visible wavelength range, where formaldehyde and NO_2 are analyzed.[22,23] Data from May 2018 onward are publicly available (formaldehyde, 10.5270/S5P-tjlxfd2 NO_2, 10.5270/S5P-s4ljg54). Here, we use version 1 of the level 2 reprocessed and offline formaldehyde[24] and tropospheric NO_2[25] vertical column densities (VCDs) from 1 May 2018 to 29 February 2020. Formaldehyde VCDs from daily orbit files are gridded on a rectilinear latitude/longitude grid with a resolution of 0.1° × 0.125°, whereby the overlap of the satellite's ground pixel corners with the grid boxes is used to generate weighted averages. To save computation time, NO_2 VCDs that were previously gridded to 0.025° × 0.025° with the same method[13] were integrated to match the coarser formaldehyde resolution. Only data with recommended quality assurance are used (0.5 for formaldehyde and 0.75 for NO_2). Note that TROPOMI formaldehyde columns are reported to be biased low by 25% for columns larger than 0.8 × 10^{16} molecules cm^{-2}.[26] However, none of the conclusions drawn in our study are impacted by this low bias, except where explicitly noted.

2.3. WRF-Chem and FOG. The Weather Research and Forecasting model coupled with Chemistry (WRF-Chem) simulates emissions, mixing, and chemical transformation of trace gases and aerosols simultaneously with meteorology. Emissions from oil and natural gas production are constrained by the fuel-based inventory of oil and gas (FOG),[27] which has recently been expanded to include VOC emissions.[3] The calculation of FOG NO_x emissions is based on reported fuel consumption and flare count observations. VOC emissions are scaled from NO_x and based on observationally derived scaling factors from aircraft tracer−tracer ratios relative to methane.[3] Note that FOG oil and gas VOC emissions do not include primary formaldehyde because formaldehyde to methane ratios cannot be used to estimate primary formaldehyde emissions without accounting for photochemical aging. Annual averages of FOG NO_x and VOC emissions are used as input to the WRF-Chem simulation and presumed to be constant over a 24 h cycle. Further WRF-Chem input emission sources include the fuel-based inventory of vehicle emissions (FIVE) for mobile sources[28] and power plant emissions based on stack monitoring data from the continuous emission monitoring systems. Other point and area sources are from the National Emissions Inventory (NEI 2017). All anthropogenic sources, except FOG, include primary formaldehyde estimates with diurnal variations based on activity rates. Biogenic emissions come from the Biogenic Emissions Inventory System (BEIS) v3.14.[29] To decrease computation time, WRF-Chem utilizes the RACM-ESRL-VCP scheme,[30] where ≥ C3 VOCs are lumped into HC3, HC5, and HC8 bins.

For comparison with TROPOMI, WRF-Chem output was interpolated from a 12 × 12 km^2 grid in a Lambert Conformal projection onto a rectilinear latitude/longitude grid of 0.1° × 0.125°. Tropospheric VCDs were calculated from WRF-Chem formaldehyde concentration profiles that were then convolved with the TROPOMI kernels and filtered to match the daily TROPOMI data coverage.

2.4. F0AM. The Framework for 0-D Atmospheric Modeling (F0AM) is a MATLAB program for simulating atmospheric chemistry.[31] F0AM is an open source software and freely available (https://github.com/AirChem/F0AM). For our 0-D model calculations, we use the following chemical mechanisms available in F0AM: the Master Chemical Mechanism (MCM), version 3.3.1,[32−36] and the Regional Atmospheric Chemistry Mechanism, version 2 (RACM2).[37] The latter is comparable to the chemical scheme used in WRF-Chem. Further details on the model setup are given in Section 3.4 below.

2.5. Industrial Activity Data. Oil and gas production data are from the Enverus DrillingInfo database. Production volumes are reported monthly for individual well locations and are gridded here to match the TROPOMI formaldehyde maps. Flared gas volumes are derived from the Visible Infrared

https://doi.org/10.1021/acsearthspacechem.3c00203
ACS Earth Space Chem. XXXX, XXX, XXX−XXX

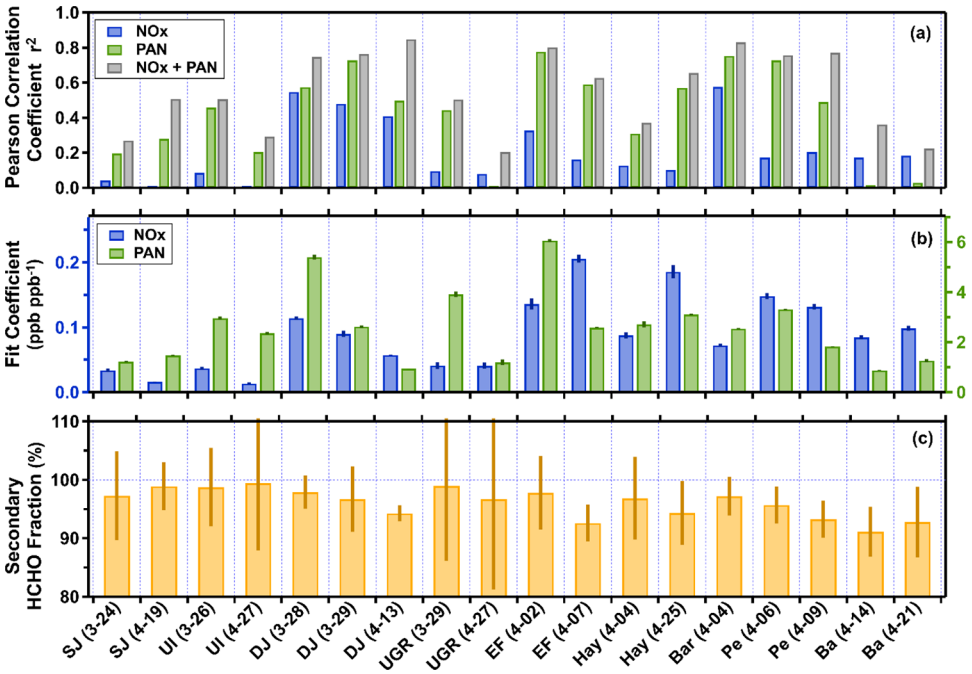

Figure 3. Fit results for all analyzed oil and natural gas basins: San Juan (SJ), Uintah (UI), Denver-Julesburg (DJ), Upper Green River (UGR), Eagle Ford (EF), Haynesville (Hay), Barnett (Bar), Permian (Pe), and Bakken (Ba). Individual flight dates are included in parentheses. (a) Pearson correlation coefficients r^2 for linear and multivariate fits. (b) Multivariate fit coefficients with fit errors for NO_x and PAN. (c) Fractional contribution of PAN to the modeled HCHO above the background, which is indicative of secondary HCHO formation in the atmosphere. Here, the error bars are the combined NO_x and PAN relative fit errors.

Imaging Radiometer Suite (VIIRS) satellite shortwave and near-infrared data.[38] Flare locations, flared gas volumes, and detection frequency are publicly available (10.3334/ORNLDAAC/1874). Flare counts calculated for our study area are weighted by their detection frequency.

2.6. Meteorological Data. Meridional and zonal wind components at 100 m above ground as well as boundary layer heights are from the ERA-5 reanalysis from the European Centre for Medium-Range Weather Forecasts (ECMWF).[39] These data are publicly available. ERA-5 data have an hourly temporal resolution and a spatial resolution of 0.25° × 0.25° latitude/longitude. For the TROPOMI data analysis in Section 3.2, hourly wind components are interpolated in space and time to match the formaldehyde spatial grid and the TROPOMI overpass time. For the box model analysis in Section 3.6, we first averaged winds and boundary layer heights over 6 h around local noon and then created seasonal averages from those data while keeping the original spatial resolution.

3. RESULTS AND DISCUSSION

3.1. Analysis of SONGNEX Formaldehyde Measurements. Formaldehyde data from the flight on 6 April 2015 in the Permian Basin are shown in Figure 2. Formaldehyde was found to be enhanced in the boundary layer parts of the flight (gray-shaded areas) to mixing ratios of ∼1.5 ppbv. To gain insight into the sources of formaldehyde, the data in Figure 2 are compared with acetyl peroxy nitrate (also commonly referred to as peroxy acetyl nitrate or PAN), as an example of a compound with a photochemical source, i.e., a secondary source, and with NO_x, as an example of a compound with a combustion source, i.e., a primary source. While formaldehyde and PAN were broadly enhanced in the boundary layer, the NO_x data showed a lot of variability when the aircraft sampled downwind from a nearby source. Clearly, formaldehyde was found to be correlated much better with PAN (Figure 2b) than with NO_x (Figure 2c), suggesting that formaldehyde's photochemical source is larger than its primary emission source.

Correlations between formaldehyde, PAN, and NO_x were calculated for all SONGNEX flights. The results are displayed in Figure 3a (see Figure S1 for average formaldehyde, PAN, and NO_x data). In 15 of 18 cases, formaldehyde was more strongly correlated with PAN, indicating a larger photochemical source for these basins as well. In the Upper Green River (UGR) on 27 April and in the Bakken (Ba) basin, formaldehyde correlated more strongly with NO_x than with PAN, but the degree of correlation was low in all three cases. It is notable that on flights in the Denver-Julesburg (DJ) and Barnett (Bar) areas, the correlation between formaldehyde and NO_x was higher and more similar to the correlation with PAN than on other flights. Both regions are near large metropolitan areas, Denver and Dallas-Fort Worth, respectively, where urban emissions are mixed with the emissions from oil and gas production. These two areas were also characterized by above average NO_x (Figure S1).

Generally, the poorer correlation between formaldehyde and NO_x is driven by high NO_x points in fresh emission plumes (e.g., Figure 2c). We can make use of this fact to separate primary and secondary sources of formaldehyde by fitting NO_x and PAN simultaneously in a multivariate fit. PAN serves as the predictor for photochemical formaldehyde formation and NO_x as the predictor for primary formaldehyde emissions. Given that mobile measurements, such as the SONGNEX aircraft observations, sample several fresh plumes, the fraction that correlates with NO_x should mostly correspond to primary formaldehyde emissions in fresh plumes, while any influence of NO_x on VOC oxidation rates should be captured by the correlation with PAN. In the multivariate fit, the measured

https://doi.org/10.1021/acsearthspacechem.3c00203
ACS Earth Space Chem. XXXX, XXX, XXX−XXX

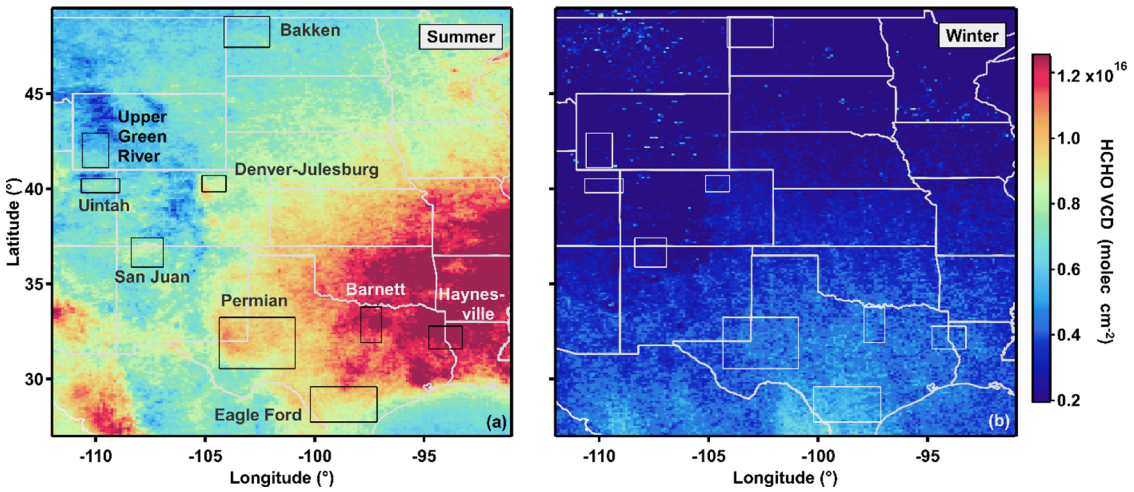

Figure 4. Average TROPOMI formaldehyde VCDs for (a) summer (June to August 2018 and 2019) and (b) winter (December to February 2018/2019 and 2019/2020). The outlined boxes denote the oil and gas production areas probed by the SONGNEX campaign.

formaldehyde is simulated by a fitted background and fitted fractions of the measured PAN and NO_x data. The formaldehyde background is estimated by a fifth-order polynomial as a function of time to account for subbasin scale variations. The results are shown in Figure 3, and an example of a multivariate fit is provided in Figure S2.

The combined fitting of PAN and NO_x leads to a better description of the observed formaldehyde, as indicated by the increased correlation coefficients across all basins (Figure 3a). The derived fit coefficients for PAN and NO_x in Figure 3b show a high degree of variability across basins. The variability in the PAN fit coefficient is likely caused by changes in atmospheric (photo) chemical activity, temperature, and the mix of precursor VOCs, while the NO_x fit coefficient is sensitive to the number, magnitude, and composition of fresh emission plumes that were sampled during a particular flight. Further differences between basins and flight days could be due to changes in local background concentrations that might not be adequately captured by the fitted background fraction and potential changes in emission sources. Using the fit coefficient results, we calculated the secondary fraction of HCHO, defined by the term proportional to PAN and divided by the sum of the terms proportional to PAN and NO_x. The derived fractions are shown in Figure 3c. They are on average (96 ± 3)% and range between 91.1% (Ba 4−14) and 99.6% (UI 4−27). In several basins, the fractions were 100% within the error margins. The displayed error bars are the combined relative errors of the PAN and NO_x fit coefficients, where larger uncertainties are mostly driven by small NO_x coefficients. Overall, these fractions are consistent despite differences in atmospheric composition and chemistry between basins and flight days. These fit results indicate that the majority of formaldehyde measured during the SONGNEX campaign does not originate from primary sources but is formed in the atmosphere as a secondary product. The SONGNEX data were recorded during March and April, where photochemical activity is still relatively low. Larger primary fractions are expected during winter and even lower fractions during summer, which will be further discussed in Section 3.6 below.

3.2. Analysis of TROPOMI Formaldehyde Measurements. While the SONGNEX campaign provided a detailed picture of the chemical composition over oil and natural gas production areas in early spring (March and April), satellite measurements capture trace gas distributions over prolonged periods of time. Figure 4 shows the TROPOMI formaldehyde vertical columns, separated into summer (June, July, and August) and winter (December, January, and February) data. For each season, daily vertical columns were averaged over 3 months and, to improve signal to noise, for 2 years, 2018 and 2019. Winter data includes January and February of the respective following year.

Formaldehyde columns during the summer are significantly higher than those during the winter, indicative of the fact that most of the formaldehyde during the summer comes from secondary production. The largest summer VCDs are found over the forested southeast United States, where large biogenic isoprene emissions lead to formaldehyde formation. Gradients over mountainous areas in the western part of the United States are mostly caused by changes in surface altitude, including those visible in the San Juan Basin. None of the outlined oil and gas production areas show a significant increase in formaldehyde columns that correlates with oil and natural gas production except for the Permian Basin during summer. Possible reasons for the lack of significant HCHO signals over other study regions are foremost the differences in total emissions. For large production regions, such as Eagle Ford in Texas, the oil- and gas-related formaldehyde signal is likely drowned out by the high background, while for the Bakken Basin, the farthest north of the study region, atmospheric conditions might only allow for comparatively slower photochemistry or higher wind speeds could lead to lower concentrations at the same level of emissions. The lack of significantly increased columns in any of the production areas during winter, when most photochemical formation is slow, means that any primary formaldehyde emissions are below the satellite's detection sensitivity. As a reference, spring and fall formaldehyde VCDs are provided in Figure S3.

To investigate whether the summer TROPOMI formaldehyde signal over the Permian Basin is related to VOC and/or NO_x emissions from oil and gas production activity, we looked at the spatial correlation between the formaldehyde vertical columns and oil and gas production volumes for the same time period. For comparison, we include TROPOMI NO_2 measurements as a tracer for primary emissions from oil and gas production. Prior studies have shown that satellite

https://doi.org/10.1021/acsearthspacechem.3c00203
ACS Earth Space Chem. XXXX, XXX, XXX−XXX

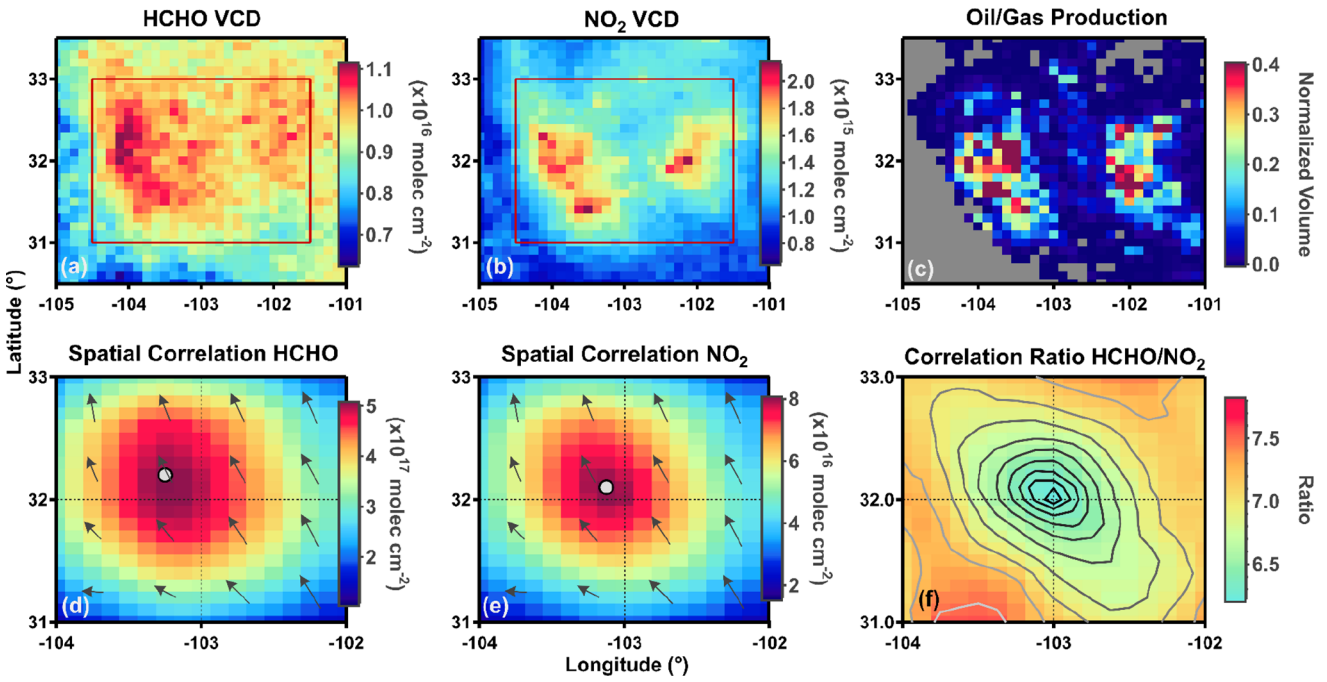

Figure 5. Spatial correlation analysis of summer formaldehyde and NO_2 VCDs with oil and gas production volumes. The top row shows the correlation analysis input: (a) formaldehyde VCDs, (b) NO_2 VCDs, and (c) normalized oil and gas production volumes. The red boxes in panels (a) and (b) indicate the cut-out that was used for cross-correlation with the total area of oil and gas production shown in panel (c). (d–f) Results of the spatial correlation analysis (see text for more details). The points in panels (d) and (e) show the location of maximum spatial correlation, while the arrows indicate the ECMWF wind vectors at 100 m above ground.

NO_2 VCDs over the Permian Basin are correlated with oil and gas production activities since the mid-2000s[40−43] and can even be used to infer oil- and gas-related NO_x emissions.[13,14] The summer averages 2018/2019 for formaldehyde, NO_2, and oil and gas production are shown in Figure 5a−c. Here, oil and gas production volumes are averaged on a grid that matches the satellite data. Since oil and gas production volumes are reported in different units, we first normalized each commodity to one by division with its respective maximum over the chosen area and then calculated the average shown in Figure 5c.

To analyze spatial correlations, we chose an area containing the highest levels of formaldehyde and NO_2 VCDs, which is outlined in red in Figure 5a,b. For the correlation analysis, the selected areas were shifted pixel by pixel in all directions across the complete oil and gas production map shown in panel (c). The result is a 2D matrix containing the sum of the product of the overlapping regions for each shifted pixel position. This so-called spatial cross-correlation analysis was performed with the signal.correlate2d function from the Python module SciPy (https://docs.scipy.org/doc/scipy). The results for formaldehyde and NO_2 are shown in Figure 5d,e and are centered on the input VCD maps, as indicated by cross hairs. Since the normalized oil and gas production is unitless, the cross-correlation results have the same units as the VCDs. Both spatial correlation results show a distinct maximum (white points in panels (d) and (e)) near the center and a mostly symmetrical drop-off in all directions. This pattern indicates a high degree of spatial correlation of both trace gases with oil and gas production and supports that increased formaldehyde VCDs over the Permian Basin are indeed related to emissions from oil and gas activities. The shift of the correlation maxima to the northwest is caused by atmospheric transport and follows the prevailing wind direction (arrows in Figure 5d,e). The relatively quick drop-off in the correlations is caused by the short atmospheric lifetimes of formaldehyde and NO_2 of just a few hours during the summer. The chemical loss away from the source locations superimposes an exponential decay signal on the correlation results. But the fact that we are using oil and gas production volumes as proxy for emissions does not allow for a quantitative derivation of atmospheric lifetimes from these results.

The formaldehyde correlation maximum is located farther downwind than that of NO_2. To assess the differences between the two correlation results, we looked at the ratio of the formaldehyde to NO_2 cross-correlation, as shown in Figure 5f. Despite being skewed into the prevailing wind direction, the ratio increases from the center outward in all directions, illustrating that the spatial correlation of NO_2 with the locations of oil and gas production is tighter than that of formaldehyde. The tighter correlation of the NO_2 concentration is consistent with primary NO_x emissions. On any given day, NO_2 columns will build up over the source area and decrease downwind due to chemical loss. In contrast, the broader spatial correlation of formaldehyde is consistent with secondary formation in the atmosphere from oil and gas precursor VOCs, which continues to increase formaldehyde columns downwind until the chemical loss becomes greater than the formation. The difference in the location of the respective correlation maxima (white points in Figure 5d,e) can provide a constraint on the average time delay between maximum NO_2 and maximum formaldehyde columns downwind: assuming a comparable atmospheric lifetime for both gases and using the average wind speed and direction, as displayed by the arrows in Figure 5d,e, yields an additional atmospheric processing time of 1.4 h before formaldehyde columns become dominated by chemical loss.

https://doi.org/10.1021/acsearthspacechem.3c00203
ACS Earth Space Chem. XXXX, XXX, XXX−XXX

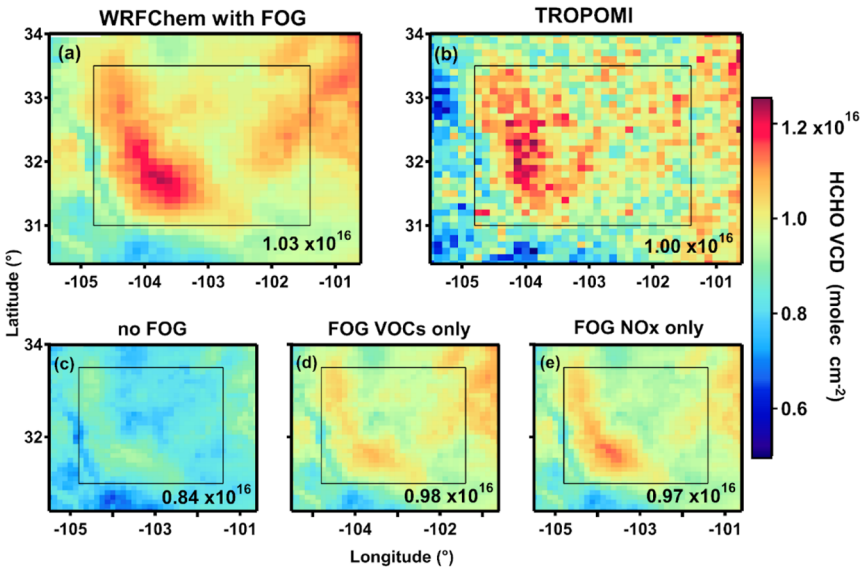

Figure 6. Formaldehyde VCDs over the Permian Basin for 10 July to 16 August 2018 (a) simulated by WRF-Chem including the FOG inventory NO_x and VOC emissions, (b) measured by TROPOMI and (c−e) WRF-Chem sensitivity studies. The numbers in each panel denote the average formaldehyde VCD in molecules cm^{-2} for the area marked by a black box.

3.3. Analysis of WRF-Chem Model Output. We simulated formaldehyde concentrations over the Permian Basin with the chemistry-transport model WRF-Chem, using our recently reported FOG inventory emission estimates of NO_x and VOCs from oil and gas production.[3] These WRF-Chem simulations were run with full chemistry across the continental United States, including other sources of NO_x and VOCs (see Section 2.3), and for the time period of 10 July to 16 August 2018. The results are shown as VCDs next to TROPOMI formaldehyde columns of the same time period in Figure 6a,b. WRF-Chem and TROPOMI are in excellent agreement. Their respective average VCDs across the Permian Basin (black outlines in Figure 6) are virtually identical and still within about 20% when assuming a 25% underestimation of the TROPOMI formaldehyde columns.[26] This result indicates that formaldehyde formation from oil and gas emissions is well described in WRF-Chem when oil and gas emissions are constrained by the FOG inventory. It also reaffirms that most observed formaldehyde over the Permian Basin during spring and summer is correlated to oil and gas production and comes from secondary sources.

To test the sensitivity of formaldehyde formation to oil and gas NO_x and VOC emissions separately, WRF-Chem was run three more times in a sensitivity study: (1) a base case that excludes FOG emissions, (2) a model run with FOG VOC emissions only, and (3) a model run with FOG NO_x emissions only. All sensitivity studies included NO_x and VOC emissions from other sources. The results are displayed in Figure 6c−e. Case 1 (Figure 6c, no FOG) quantifies the formaldehyde without local oil and gas NO_x and VOC emissions and shows that inclusion of those emissions (Figure 6a, with FOG) adds on average about 2×10^{15} molecules cm^{-2} to the formaldehyde column, which is about 0.5 ppb for a well-mixed, typical summer boundary layer height of 1.8 km. The second and third cases produce formaldehyde yields that are comparable to the full FOG case, adding on average 1.4×10^{15} molecules cm^{-2} (Figure 6d) and 1.3×10^{15} molecules cm^{-2} (Figure 6e) to the tropospheric column, respectively. In the second case (FOG VOCs only), additional formaldehyde is formed from oil and gas VOC emissions in the presence of NO_x from other sources, while in the third case (FOG NO_x only), additional formaldehyde is formed from VOCs from other sources in the presence of oil and gas NO_x. Interestingly, both scenarios produce almost identical formaldehyde, which suggests that the local emissions in the Permian Basin are in a transition regime between being NO_x and VOC limited. These results highlight the importance of understanding both oil and gas VOC and NO_x emissions in order to correctly simulate VOC oxidation chemistry in atmospheric models, e.g., for air quality analysis. The implication for secondary formaldehyde formation is that both VOC and NO_x emissions from oil and gas production are equally important.

3.4. Evaluation of Chemical Mechanisms. The chemical mechanism utilized in WRF-Chem is optimized for the simulation of urban pollution with faster reacting VOCs (alkenes, aromatics, and higher alkanes). VOC emissions from oil and gas production, however, contain several slower reacting VOCs, especially smaller alkanes and aromatics. Therefore, the formation of formaldehyde from these precursors may not be adequately represented in WRF-Chem. To test the ability of the WRF-Chem chemical mechanism to accurately describe formaldehyde formation from oil and gas VOCs, we used 0-D model calculations with the Master Chemical Mechanism (MCM), which has explicit VOC reaction schemes, and tested it against 0-D model calculations with the Regional Atmospheric Chemistry Mechanism, version 2 (RACM2), the latter being comparable to the WRF-Chem chemical mechanism. As input, we used trace gas and ambient condition measurements from the SONGNEX Permian Basin flight on 6 April 2015 (Figure 2). Boundary layer averages for the measured species are given in Table 1. The average temperature, pressure, relative humidity, and solar zenith angle are 867 hPa, 293° K, 31%, and 40°, respectively. Note that high-quality data of propene, an efficient formaldehyde precursor, was not available for SONGNEX. For subsequent discussion, measured VOCs in Table 1 are separated into different source categories according to their main emission sources: biogenic, emissions from

https://doi.org/10.1021/acsearthspacechem.3c00203
ACS Earth Space Chem. XXXX, XXX, XXX−XXX

Table 1. 0-D Modeling Input

VOC source	compound	mixing ratio (ppbv)	
	O_3	45.01	
	NO	0.10	
	NO_2	0.30	
biogenic	isoprene	0.0080	
	alpha-pinene	0.0016	
combustion	acetaldehyde	0.60	
	ethene	0.11	
other	acetone	1.66	
	MEK	0.30	
	ethanol	0.47	
	methane (BG)[a]	1857.77	
oil and gas	methane (OG)[a]	68.84	
	ethane	9.30	
	benzene	0.098	
	o-xylene	0.0042	
	m-xylene[b]	0.0058	
	p-xylene[b]	0.0058	
		MCM	RACM2 (group name)
	propane	6.06	10.15 (HC3)
	n-butane	3.07	
	isobutane	1.02	
	isobutane	0.72	1.84 (HC5)
	n-hexane	0.20	
	n-pentane	0.85	
	n-heptane	0.066	
	n-octane	0.024	0.108 (HC8)
	cyclohexane	0.084	
	toluene	0.053	0.063 (Tol)
	ethylbenzene	0.010	

[a]Methane is separated into a background (BG) and oil and gas (OG) source by applying a 10th percentile background correction to the total measured methane. [b]Measured combined and split evenly for model input.

combustion processes, other sources, and fugitive or venting VOC emissions from oil and gas production. Methane is separated into a local oil and gas and other (background) source due to its high background levels. For simplicity, we refrain from background corrections of other trace gases, such as acetaldehyde, or including source attributions for reaction products, such as acetone and MEK, which can also be formed from the oxidation of oil and gas VOCs.

Using F0AM (Section 2.4), the formaldehyde yield is simulated separately for each individual input VOC (MCM and RACM2) or VOC group (RACM2) over 6 h at a constant OH concentration of 2×10^6 molecules cm^{-3} while keeping the inorganic species constrained. The model results are shown in Figure 7. Here, the oil and gas (OG) source emission category is separated into "individuals", which contain VOCs that have their individual reaction scheme in both MCM and RACM2, while "grouped" contains the VOCs that are lumped in RACM2 (Table 1).

As expected, the formaldehyde amounts simulated by individual chemical reaction schemes, i.e., all categories but "OG grouped", are comparable in both the MCM and RACM2 chemical mechanisms. The formaldehyde yield for the grouped species, however, differs. Formaldehyde produced from the HC3 group in RACM2 is almost double the sum of the individual species in MCM, while the formaldehyde yield for higher carbon numbers is comparable to that of MCM. The smaller alkanes from oil and gas production are clearly not well represented by the lumped mechanism. The overestimated formaldehyde yield from the HC3 group is compounded by the fact that the HC3 alkanes make up 81.1% of the grouped species here. In total, however, the fraction of formaldehyde produced from grouped species is 26.3% for RACM2 and 17.9% for the matching compounds in MCM and the combined fractional formaldehyde yield from "OG individuals" and "OG grouped" is 30.0% for RACM2 and 22.3% for MCM. Since most of the oil and gas production activities in the Permian Basin are in remote areas, we can assume that the

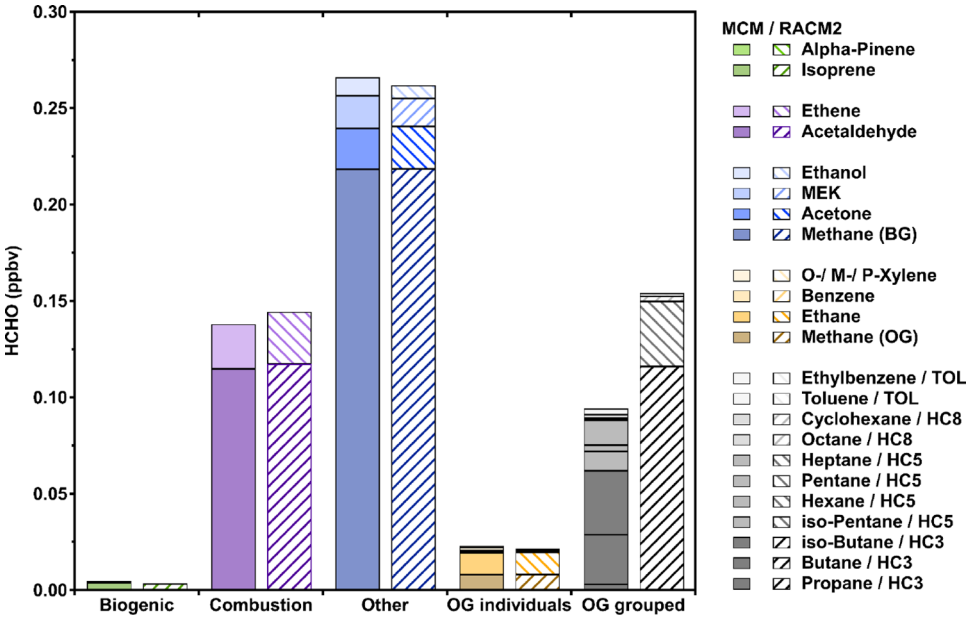

Figure 7. 0-D formaldehyde modeling results using the MCM and RACM2 chemical mechanisms with input VOCs measured over the Permian Basin on 6 April 2015. The legend follows the stacked bars in the graph top to bottom. Xylenes are simulated separately in both mechanisms, but their formaldehyde yield is so small that they have the same color code.

https://doi.org/10.1021/acsearthspacechem.3c00203
ACS Earth Space Chem. XXXX, XXX, XXX−XXX

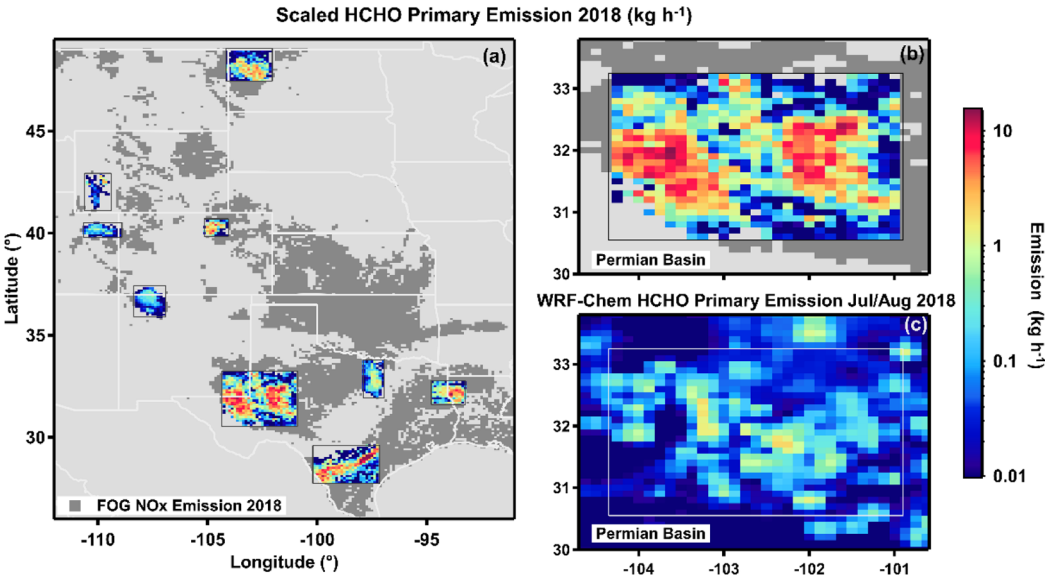

Figure 8. Primary formaldehyde emissions scaled from FOG NO_x emissions for the year 2018 for (a) all study areas and (b) the Permian Basin. (c) Formaldehyde emissions used in WRF-Chem simulations (Section 3.3). Emissions shown in panel (c) are weekday emissions averaged over 6 h around local noon.

majority of VOCs from combustion sources are related to oil and gas activities. If, for example, we attributed 70% of combustion VOCs to the oil and gas sector, then the fractional formaldehyde yield from oil- and gas-related VOC emissions rises to 47.3% for RACM2 and 40.6% for MCM. These results show that the impact of overestimated formaldehyde from the HC3 group in the RACM2 mechanism is determined by the fraction of HC3 VOCs to total VOCs as well as by the amount of precursor VOCs that are attributed to oil and gas activities. Here, the total difference is less than 10 percentage points. More broadly, these model results suggest that in the Permian Basin, secondary formaldehyde sources are mostly evenly spread between combustion and fugitive oil and gas sources. Within the combustion sources, acetaldehyde produces by far the largest amount of formaldehyde, while for fugitive sources, the largest formaldehyde fractions come from butanes/HC3.

3.5. Estimation of Primary Formaldehyde Emissions. Insufficient knowledge of primary formaldehyde creates uncertainties when trying to model ozone formation from oil and gas emissions in air quality simulations.[7,44] Separating primary from secondary formaldehyde in atmospheric measurements typically presents a challenge since daytime formaldehyde concentrations are often overwhelmingly from secondary formation. Here, we constrain primary formaldehyde emissions based on the SONGNEX data analysis (Section 3.1) as follows: using NO_x emissions from the FOG inventory (Section 2.3) as a tracer, direct formaldehyde emissions from oil and gas production are estimated by scaling FOG NO_x to formaldehyde with the NO_x multivariate fit coefficients (Figure 3b). To do so, we first averaged individual NO_x fit coefficients for each basin (Figure S4) and then scaled FOG NO_x emissions for the years 2018 to 2020 with the averaged fit coefficients within each SONGNEX study area. Spatial distributions of primary formaldehyde emission estimates are shown in Figure 8 for 2018 (see Figure S5 for 2019 and 2020). Spatial averages and sum totals are calculated for each study area and presented in Figure S6. Averages per basin range from 0.07 to 2.2 kg h^{-1}, while annual sum totals are between 8.6 and 1463 kg h^{-1} (San Juan, 2019, and Permian Basin, 2019, respectively; see Figure S6). Within the Permian Basin study area (Figure 8b), the average/maximum for the scaled formaldehyde emissions in 2018 are 1.63/15.21 kg h^{-1} (equivalent to 0.25/2.33 × 10^{14} molecules h^{-1} cm^{-2}). The magnitude of these emissions is comparable to primary formaldehyde emissions of 1.1 × 10^{14} molecules h^{-1} cm^{-2} reported for urban areas in the northeast United States.[45] Figure 8c shows the primary formaldehyde emissions used in the WRF-Chem simulations (Section 3.3) that come from other sources. For the Permian Basin study area, the average is 0.13 kg h^{-1}, which is about 1 order of magnitude smaller than the estimated primary emissions from oil and gas production. This difference could point to the fact that a significant fraction of formaldehyde is missed when direct emissions from oil and gas production are not accounted for.

In oil and gas production regions, flaring can be a significant additional source of combustion-related emissions. For example, NO_x emissions from flaring were estimated to contribute 6% to the total oil and gas NO_x emissions in the Permian Basin in 2015[3,42] and 5% in 2018. To get an estimate on how much flaring contributes to primary formaldehyde emissions, we calculated annual flare counts for the Permian Basin study area in 2018 and applied an emission factor range of 0.35 to 0.79 kg h^{-1} per flare based on reported measurements[46] (see Section S1 for further details). The resulting average formaldehyde emissions from flaring are 0.09 to 0.2 kg h^{-1}, which is equivalent to 5 to 12% of the total primary emissions for the Permian Basin study area in 2018. This result is consistent with the magnitude of our total primary formaldehyde estimate, and the fractional formaldehyde contribution coming from flaring is highly comparable to that of NO_x.

3.6. Primary vs Secondary Formaldehyde. To get a sense of how our primary formaldehyde estimates compare to observations, we applied a simple box model to simulate average seasonal formaldehyde abundances from primary emissions for the Permian Basin study area for 2018 and 2019. Primary formaldehyde VCDs and mixing ratios were calculated based on our emission estimates, ECMWF wind

https://doi.org/10.1021/acsearthspacechem.3c00203
ACS Earth Space Chem. XXXX, XXX, XXX−XXX

Table 2. Box Model Results for Primary Formaldehyde Emissions

season	HCHO primary emission (kg h^{-1})	HCHO chemical lifetime (h)	wind speed (m/s)	PBL height (km)	HCHO VCD (molecules cm^{-2})	HCHO mixing ratio (ppbv)
Mar−May 2018	1.63	4	3.0	1.74	0.87×10^{14}	0.023
Jun−Aug 2018	1.63	2	3.8	1.84	0.48×10^{14}	0.012
Sep−Nov 2018	1.63	4	1.2	0.96	0.97×10^{14}	0.045
Dec−Feb 2018/2019	1.63	8	2.5	0.88	1.52×10^{14}	0.077
Mar−May 2019	2.19	4	2.7	1.49	1.17×10^{14}	0.036
Jun−Aug 2019	2.19	2	2.8	1.80	0.65×10^{14}	0.016
Sep−Nov 2019	2.19	4	2.3	1.22	1.19×10^{14}	0.044
Dec−Feb 2019/2020	2.19	8	2.3	0.84	2.07×10^{14}	0.112

fields, and planetary boundary layer (PBL) heights averaged over 6 h around local noon and assumed seasonally dependent, daytime chemical lifetimes. See Section S2 and Figure S7 for further details. The results are reported for steady-state conditions in Table 2. For easier comparison, winter calculations (Dec−Feb) use emissions from December.

As expected, simulated primary formaldehyde abundances are smallest in summer (Jun−Aug) and largest in winter (Dec−Feb) due to the shortest and longest chemical lifetimes, respectively. The magnitude of the modeled primary formaldehyde mixing ratios is between 0.012 ppbv for the summer and 0.112 ppbv for winter. Taking the above background average formaldehyde measured during SONGNEX over the Permian Basin as a reference yields primary formaldehyde fractions of 4.6 and 7.2% for the simulated 2018 and 2019 spring mixing ratios, which is very consistent with the primary formaldehyde fraction of 5.5% derived for the Permian Basin above (Figure 3c). These results support our earlier conclusions that only a small fraction of boundary layer formaldehyde comes from primary sources. This fraction, however, is seasonally dependent, as illustrated by the box model results. The fraction of primary formaldehyde will be even lower during the summer, when atmospheric photochemistry is most active. During winter, though, the fractional contribution of primary formaldehyde could be significantly higher. Around 25% has been simulated for urban areas during winter.[47] Increases in primary fractions during winter can be especially expected for shallow boundary layers under meteorological inversion conditions and, given the emission gradients across the Permian Basin area (Figure 8b), for locations closer to strong emission sources. The box model simulated primary formaldehyde VCDs are about 1 to 2 orders of magnitude smaller than the TROPOMI observation (see Figures 4 and 6), which renders signals from primary formaldehyde emissions below the satellite's detection limit, even during winter.

4. SUMMARY AND CONCLUSIONS

We have examined sources of formaldehyde in U.S. oil and gas production regions, using in situ aircraft measurements from the SONGNEX campaign, TROPOMI satellite data, and WRF-Chem modeling output. The analyses of aircraft and satellite data consistently showed that most of the increased formaldehyde observed over oil and gas production regions during the spring and summer is the product of secondary formation in the atmosphere. For the SONGNEX campaign, we found that across nine different oil and gas basins in the United States, an average of (96 ± 3)% of above background formaldehyde comes from secondary sources during April and March. Spatial correlation analysis of TROPOMI formaldehyde and NO_2 columns over the Permian Basin showed that increased formaldehyde VCDs during summer correlate with the locations of oil and gas production. The farther downwind shifted spatial correlation maximum of formaldehyde compared to NO_2 is consistent with secondary formation in the atmosphere from oil and gas precursor VOCs, while NO_2 comes from primary sources.

Our work provides a constraint on primary formaldehyde by demonstrating that its emissions can be scaled using oil- and gas-related NO_x emissions as described by the FOG NO_x inventory. Good consistency was found between our scaled emissions and SONGNEX aircraft measurements in 2015, which supports the fact that our method of scaling formaldehyde emissions to NO_x emissions is a good representation of oil- and gas-related primary formaldehyde emissions. We conclude that for spring through fall of any given year, primary formaldehyde emissions from oil and gas production will contribute significantly less than 10% to the total boundary layer formaldehyde. During winter, though, this fraction could be higher, especially for shallow boundary layers and under meteorological inversion conditions. Future work could include adding oil- and gas-related primary formaldehyde emissions into the FOG inventory.

WRF-Chem modeled formaldehyde columns compared very well to TROPOMI formaldehyde observations when oil and gas NO_x and VOC emissions from the FOG inventory were included, indicating that the FOG inventory provides a good description of oil and gas emissions. Sensitivity studies on the impact of oil- and gas-related emissions on secondary formaldehyde formation illustrated that NO_x emissions from oil and gas are equally important to oil and gas VOC emissions in order to get the total VOC oxidation budget right. This is especially relevant for air quality studies that simulate ozone formation but also affects air pollution mitigation strategies. For example, controlling NO_x emission in order to reduce ozone has a significant cobenefit in reducing (toxic) formaldehyde as well.[48]

Based on the 0-D modeling study comparing MCM with RACM2, we found that smaller alkanes from oil and gas production are not well represented by the lumped VOC mechanism in RACM2, as used in WRF-Chem. The formaldehyde yield from the HC3 group in RACM2 was almost double that of the respective individual species in MCM. However, the impact of this overestimation on the total formaldehyde yield from secondary production is much smaller, in our case less than 10 percentage points, and depends on the relative contribution of HC3 VOCs to the total amount of oil- and gas-related precursor VOCs. Going forward,

https://doi.org/10.1021/acsearthspacechem.3c00203
ACS Earth Space Chem. XXXX, XXX, XXX−XXX

understanding the relative importance of individual VOCs in formaldehyde formation and accounting for their abundance could help mitigate the effect of lumping oil and gas VOCs in chemical mechanisms. Based on our case study, butane and isobutane produced about 95% of the formaldehyde in the HC3 group. Having explicit mechanisms for these species could help reduce the overproduction of formaldehyde in this group. Alternatively, product yields in the HC3 group mechanisms could be scaled down when working with oil and gas VOCs.

With respect to understanding and tracking oil and gas VOC emissions, we found that hydrocarbons released from oil and gas activities are important precursors to formaldehyde, but other VOC sources contribute as well. The total budget of secondary formaldehyde formation is highly sensitive to NO_x. As a result, modeling of formaldehyde over oil and gas regions needs to consider oil and gas hydrocarbons as well as oil and gas NO_x emissions, but observing formaldehyde by itself is not an unambiguous proxy for oil and gas hydrocarbon emissions.

TROPOMI also measures glyoxal, another VOC that is formed in the atmosphere from precursor VOCs. Theoretically, a similar analysis could be performed with glyoxal measurements in oil and gas production regions. However, the glyoxal yield from our 0-D MCM modeling study (Section 3.4) is 0.005 ppbv, which is well below the satellite's detection limit.[49] Significant glyoxal signals from oil and gas production are, therefore, not expected.

For large oil and gas regions in remote areas, such as the Permian Basin, where anthropogenic emissions are mostly dominated by the oil and gas industry, future combined analysis of satellite NO_2 and formaldehyde data might be able to provide a constraint on trends over time for formaldehyde sources and add some insight into the underlying oil and gas VOC emissions. Especially, the recent successful launch of the Tropospheric Emissions: Monitoring of Pollution (TEMPO) satellite instrument, which will measure NO_2 and formaldehyde on an hourly basis and at an unprecedented spatial resolution of 2×4.5 km^2, will allow us to further monitor oil and gas emissions and, for the first time, observe the daytime chemical cycle from space.

■ ASSOCIATED CONTENT

Supporting Information

The Supporting Information is available free of charge at https://pubs.acs.org/doi/10.1021/acsearthspacechem.3c00203.

Information on primary formaldehyde from flaring, box model simulations of primary formaldehyde, and SI Figures 1−7 (Dix_et_al_HCHO_oil_gas_SI.pdf) (PDF)

■ AUTHOR INFORMATION

Corresponding Author

Barbara Dix − *Cooperative Institute for Research in Environmental Sciences, University of Colorado, Boulder, Colorado 80309, United States;* orcid.org/0000-0001-6753-8620; Email: barbara.dix@colorado.edu

Authors

Meng Li − *Cooperative Institute for Research in Environmental Sciences, University of Colorado, Boulder, Colorado 80309, United States; NOAA Chemical Sciences Laboratory, Boulder, Colorado 80305, United States*

Esther Roosenbrand − *Cooperative Institute for Research in Environmental Sciences, University of Colorado, Boulder, Colorado 80309, United States; Department of Civil Engineering and Geosciences, Technical University of Delft, Delft 2628 CN, Netherlands;* Present Address: Faculty of Aerospace Engineering, Technical University of Delft, 2628 CN Delft, Netherlands

Colby Francoeur − *Cooperative Institute for Research in Environmental Sciences and Department of Mechanical Engineering, University of Colorado, Boulder, Colorado 80309, United States; NOAA Chemical Sciences Laboratory, Boulder, Colorado 80305, United States;* orcid.org/0000-0003-4491-7462

Steven S. Brown − *NOAA Chemical Sciences Laboratory, Boulder, Colorado 80305, United States; Department of Chemistry, University of Colorado, Boulder, Colorado 80309, United States;* orcid.org/0000-0001-7477-9078

Jessica B. Gilman − *NOAA Chemical Sciences Laboratory, Boulder, Colorado 80305, United States;* orcid.org/0000-0002-7899-9948

Thomas F. Hanisco − *Atmospheric Chemistry and Dynamics Laboratory, NASA Goddard Space Flight Center, Greenbelt, Maryland 20771, United States;* orcid.org/0000-0001-9434-8507

Frank Keutsch − *Department of Chemistry, University of Wisconsin, Madison, Wisconsin 53706, United States;* Present Address: Paulson School of Engineering and Applied Science and Department of Chemistry and Chemical Biology, Harvard University, Cambridge, Massachusetts 02138, United States

Abigail Koss − *Cooperative Institute for Research in Environmental Sciences, University of Colorado, Boulder, Colorado 80309, United States; NOAA Chemical Sciences Laboratory, Boulder, Colorado 80305, United States;* Present Address: TOFWERK USA, Boulder, Colorado 80301, United States

Brian M. Lerner − *Cooperative Institute for Research in Environmental Sciences, University of Colorado, Boulder, Colorado 80309, United States; NOAA Chemical Sciences Laboratory, Boulder, Colorado 80305, United States;* Present Address: Aerodyne Research, Billerica, Massachusetts 01821, United States

Jeff Peischl − *Cooperative Institute for Research in Environmental Sciences, University of Colorado, Boulder, Colorado 80309, United States; NOAA Chemical Sciences Laboratory, Boulder, Colorado 80305, United States;* orcid.org/0000-0002-9320-7101

James M. Roberts − *NOAA Chemical Sciences Laboratory, Boulder, Colorado 80305, United States;* orcid.org/0000-0002-8485-8172

Thomas B. Ryerson − *NOAA Chemical Sciences Laboratory, Boulder, Colorado 80305, United States;* Present Address: ChampionX Emissions Technologies, The Woodlands, Texas 77381, United States

Jason M. St. Clair − *Atmospheric Chemistry and Dynamics Laboratory, NASA Goddard Space Flight Center, Greenbelt, Maryland 20771, United States; Joint Center for Earth Systems Technology, University of Maryland Baltimore County, Baltimore, Maryland 21228, United States;* orcid.org/0000-0002-9367-5749

https://doi.org/10.1021/acsearthspacechem.3c00203
ACS Earth Space Chem. XXXX, XXX, XXX−XXX

Patrick R. Veres − *Cooperative Institute for Research in Environmental Sciences, University of Colorado, Boulder, Colorado 80309, United States; NOAA Chemical Sciences Laboratory, Boulder, Colorado 80305, United States;* Present Address: Research Aviation Facility, NCAR Earth Observing Laboratory, Boulder, Colorado 80307, United States

Carsten Warneke − *Cooperative Institute for Research in Environmental Sciences, University of Colorado, Boulder, Colorado 80309, United States; NOAA Chemical Sciences Laboratory, Boulder, Colorado 80305, United States;* orcid.org/0000-0003-3811-8496

Robert J. Wild − *Cooperative Institute for Research in Environmental Sciences, University of Colorado, Boulder, Colorado 80309, United States; NOAA Chemical Sciences Laboratory, Boulder, Colorado 80305, United States;* Present Address: Institute for Ion Physics and Applied Physics, University of Innsbruck, Innsbruck 6020, Austria

Glenn M. Wolfe − *Atmospheric Chemistry and Dynamics Laboratory, NASA Goddard Space Flight Center, Greenbelt, Maryland 20771, United States;* orcid.org/0000-0001-6586-4043

Bin Yuan − *Cooperative Institute for Research in Environmental Sciences, University of Colorado, Boulder, Colorado 80309, United States; NOAA Chemical Sciences Laboratory, Boulder, Colorado 80305, United States;* Present Address: Institute of Environmental and Climate Research, Jinan University, Guangzhou 511443, China; Guangdong-Hongkong-Macau Joint Laboratory of Collaborative Innovation for Environmental Quality, Guangzhou 511443, China; orcid.org/0000-0003-3041-0329

J. Pepijn Veefkind − *Department of Civil Engineering and Geosciences, Technical University of Delft, Delft 2628 CN, Netherlands; Royal Netherlands Meteorological Institute, De Bilt 3731 GA, Netherlands*

Pieternel F. Levelt − *NCAR Atmospheric Chemistry Observations & Modeling Lab, Boulder, Colorado 80307, United States; Royal Netherlands Meteorological Institute, De Bilt 3731 GA, Netherlands; Department of Civil Engineering and Geosciences, Technical University of Delft, Delft 2628 CN, Netherlands*

Brian C. McDonald − *NOAA Chemical Sciences Laboratory, Boulder, Colorado 80305, United States;* orcid.org/0000-0001-8600-5096

Joost de Gouw − *Cooperative Institute for Research in Environmental Sciences and Department of Chemistry, University of Colorado, Boulder, Colorado 80309, United States;* orcid.org/0000-0002-0385-1826

Complete contact information is available at: https://pubs.acs.org/10.1021/acsearthspacechem.3c00203

Notes

The authors declare no competing financial interest.

■ ACKNOWLEDGMENTS

This work was financially supported by the NASA ACMAP program under award number 80NSSC19K0979. We acknowledge funding from the Rocky Mountain Institute and Blue Sky Resources. We are grateful to Enverus for providing access to the DrillingInfo database. We thank NOAA's High Performance Computing Program and NASA's Tropospheric Composition Program. We thank GEO-CAPE for supporting the formaldehyde measurements during SONGNEX. This research was funded in part by the National Science Foundation under cooperative agreement no. AGS-1755088 and in part by NOAA cooperative agreement NA17OAR4320101. KNMI contributions were funded by The Netherlands Space Office (NSO) under the TROPOMI Science Contract. This work contains modified Copernicus Sentinel 5 Precursor data 2018−2020.

■ REFERENCES

(1) Alvarez, R. A.; Zavala-Araiza, D.; Lyon, D. R.; Allen, D. T.; Barkley, Z. R.; Brandt, A. R.; Davis, K. J.; Herndon, S. C.; Jacob, D. J.; Karion, A.; Kort, E. A.; Lamb, B. K.; Lauvaux, T.; Maasakkers, J. D.; Marchese, A. J.; Omara, M.; Pacala, S. W.; Peischl, J.; Robinson, A. L.; Shepson, P. B.; Sweeney, C.; Townsend-Small, A.; Wofsy, S. C.; Hamburg, S. P. Assessment of Methane Emissions from the U.S. Oil and Gas Supply Chain. *Science* **2018**, *361* (6398), 186−188.

(2) Zhang, Y.; Gautam, R.; Pandey, S.; Omara, M.; Maasakkers, J. D.; Sadavarte, P.; Lyon, D.; Nesser, H.; Sulprizio, M. P.; Varon, D. J.; Zhang, R.; Houweling, S.; Zavala-Araiza, D.; Alvarez, R. A.; Lorente, A.; Hamburg, S. P.; Aben, I.; Jacob, D. J. Quantifying Methane Emissions from the Largest Oil-Producing Basin in the United States from Space. *Sci. Adv.* **2020**, *6* (17), No. eaaz5120.

(3) Francoeur, C. B.; McDonald, B. C.; Gilman, J. B.; Zarzana, K. J.; Dix, B.; Brown, S. S.; de Gouw, J. A.; Frost, G. J.; Li, M.; McKeen, S. A.; Peischl, J.; Pollack, I. B.; Ryerson, T. B.; Thompson, C.; Warneke, C.; Trainer, M. Quantifying Methane and Ozone Precursor Emissions from Oil and Gas Production Regions across the Contiguous US. *Environ. Sci. Technol.* **2021**, *55* (13), 9129−9139.

(4) Peischl, J.; Eilerman, S. J.; Neuman, J. A.; Aikin, K. C.; de Gouw, J.; Gilman, J. B.; Herndon, S. C.; Nadkarni, R.; Trainer, M.; Warneke, C.; Ryerson, T. B. Quantifying Methane and Ethane Emissions to the Atmosphere From Central and Western U.S. Oil and Natural Gas Production Regions. *J. Geophys. Res. Atmos.* **2018**, *123*, 7725.

(5) Edwards, P. M.; Brown, S. S.; Roberts, J. M.; Ahmadov, R.; Banta, R. M.; deGouw, J. A.; Dubé, W. P.; Field, R. A.; Flynn, J. H.; Gilman, J. B.; Graus, M.; Helmig, D.; Koss, A.; Langford, A. O.; Lefer, B. L.; Lerner, B. M.; Li, R.; Li, S.-M.; McKeen, S. A.; Murphy, S. M.; Parrish, D. D.; Senff, C. J.; Soltis, J.; Stutz, J.; Sweeney, C.; Thompson, C. R.; Trainer, M. K.; Tsai, C.; Veres, P. R.; Washenfelder, R. A.; Warneke, C.; Wild, R. J.; Young, C. J.; Yuan, B.; Zamora, R. High Winter Ozone Pollution from Carbonyl Photolysis in an Oil and Gas Basin. *Nature* **2014**, *514* (7522), 351−354.

(6) Roest, G.; Schade, G. Quantifying Alkane Emissions in the Eagle Ford Shale Using Boundary Layer Enhancement. *Atmospheric Chem. Phys.* **2017**, *17* (18), 11163−11176.

(7) Ahmadov, R.; McKeen, S.; Trainer, M.; Banta, R.; Brewer, A.; Brown, S.; Edwards, P. M.; de Gouw, J. A.; Frost, G. J.; Gilman, J.; Helmig, D.; Johnson, B.; Karion, A.; Koss, A.; Langford, A.; Lerner, B.; Olson, J.; Oltmans, S.; Peischl, J.; Pétron, G.; Pichugina, Y.; Roberts, J. M.; Ryerson, T.; Schnell, R.; Senff, C.; Sweeney, C.; Thompson, C.; Veres, P. R.; Warneke, C.; Wild, R.; Williams, E. J.; Yuan, B.; Zamora, R. Understanding High Wintertime Ozone Pollution Events in an Oil- and Natural Gas-Producing Region of the Western US. *Atmospheric Chem. Phys.* **2015**, *15* (1), 411−429.

(8) Pétron, G.; Karion, A.; Sweeney, C.; Miller, B. R.; Montzka, S. A.; Frost, G. J.; Trainer, M.; Tans, P.; Andrews, A.; Kofler, J.; Helmig, D.; Guenther, D.; Dlugokencky, E.; Lang, P.; Newberger, T.; Wolter, S.; Hall, B.; Novelli, P.; Brewer, A.; Conley, S.; Hardesty, M.; Banta, R.; White, A.; Noone, D.; Wolfe, D.; Schnell, R. A New Look at Methane and Nonmethane Hydrocarbon Emissions from Oil and Natural Gas Operations in the Colorado Denver-Julesburg Basin. *J. Geophys. Res. Atmospheres* **2014**, *119* (11), 6836−6852.

(9) Holliman, J.; Schade, G. W. Comparing Permitted Emissions to Atmospheric Observations of Hydrocarbons in the Eagle Ford Shale Suggests Permit Violations. *Energies* **2021**, *14* (3), 780.

(10) Veefkind, J. P.; Serrano-Calvo, R.; de Gouw, J.; Dix, B.; Schneising, O.; Buchwitz, M.; Barré, J.; van der, A. R. J.; Liu, M.; Levelt, P. F. Widespread Frequent Methane Emissions From the Oil and Gas Industry in the Permian Basin. *J. Geophys. Res. Atmos.* **2023**, *128* (3), e2022JD037479.
(11) Schneising, O.; Buchwitz, M.; Reuter, M.; Vanselow, S.; Bovensmann, H.; Burrows, J. P. Remote Sensing of Methane Leakage from Natural Gas and Petroleum Systems Revisited. *Atmospheric Chem. Phys.* **2020**, *20* (15), 9169−9182.
(12) Liu, M.; van der, A. R.; van Weele, M.; Eskes, H.; Lu, X.; Veefkind, P.; de Laat, J.; Kong, H.; Wang, J.; Sun, J.; Ding, J.; Zhao, Y.; Weng, H. A New Divergence Method to Quantify Methane Emissions Using Observations of Sentinel-5P TROPOMI. *Geophys. Res. Lett.* **2021**, *48* (18), e2021GL094151.
(13) Dix, B.; Francoeur, C.; Li, M.; Serrano-Calvo, R.; Levelt, P. F.; Veefkind, J. P.; McDonald, B. C.; de Gouw, J. Quantifying NO x Emissions from U.S. Oil and Gas Production Regions Using TROPOMI NO 2. *ACS Earth Space Chem.* **2022**, *6* (2), 403−414.
(14) Sun, K. Derivation of Emissions From Satellite-Observed Column Amounts and Its Application to TROPOMI NO2 and CO Observations. *Geophys. Res. Lett.* **2022**, *49* (23), No. e2022GL101102.
(15) Millet, D. B.; Jacob, D. J.; Boersma, K. F.; Fu, T.-M.; Kurosu, T. P.; Chance, K.; Heald, C. L.; Guenther, A. Spatial Distribution of Isoprene Emissions from North America Derived from Formaldehyde Column Measurements by the OMI Satellite Sensor. *J. Geophys. Res. Atmos.* **2008**, *113* (D2), D02307.
(16) USEPA*Initial List of Hazardous Air Pollutants with Modifications*.https://www.epa.gov/haps/initial-list-hazardous-air-pollutants-modifications.
(17) Warneke, C.; Trainer, M.; de Gouw, J. A.; Parrish, D. D.; Fahey, D. W.; Ravishankara, A. R.; Middlebrook, A. M.; Brock, C. A.; Roberts, J. M.; Brown, S. S.; Neuman, J. A.; Lerner, B. M.; Lack, D.; Law, D.; Hübler, G.; Pollack, I.; Sjostedt, S.; Ryerson, T. B.; Gilman, J. B.; Liao, J.; Holloway, J.; Peischl, J.; Nowak, J. B.; Aikin, K. C.; Min, K.-E.; Washenfelder, R. A.; Graus, M. G.; Richardson, M.; Markovic, M. Z.; Wagner, N. L.; Welti, A.; Veres, P. R.; Edwards, P.; Schwarz, J. P.; Gordon, T.; Dube, W. P.; McKeen, S. A.; Brioude, J.; Ahmadov, R.; Bougiatioti, A.; Lin, J. J.; Nenes, A.; Wolfe, G. M.; Hanisco, T. F.; Lee, B. H.; Lopez-Hilfiker, F. D.; Thornton, J. A.; Keutsch, F. N.; Kaiser, J.; Mao, J.; Hatch, C. D. Instrumentation and Measurement Strategy for the NOAA SENEX Aircraft Campaign as Part of the Southeast Atmosphere Study 2013. *Atmospheric Meas. Technol.* **2016**, *9* (7), 3063−3093.
(18) Cazorla, M.; Wolfe, G. M.; Bailey, S. A.; Swanson, A. K.; Arkinson, H. L.; Hanisco, T. F. A New Airborne Laser-Induced Fluorescence Instrument for in Situ Detection of Formaldehyde throughout the Troposphere and Lower Stratosphere. *Atmospheric Meas. Technol.* **2015**, *8* (2), 541−552.
(19) Koss, A.; Yuan, B.; Warneke, C.; Gilman, J. B.; Lerner, B. M.; Veres, P. R.; Peischl, J.; Eilerman, S.; Wild, R.; Brown, S. S.; Thompson, C. R.; Ryerson, T.; Hanisco, T.; Wolfe, G. M.; Clair, J. M. S.; Thayer, M.; Keutsch, F. N.; Murphy, S.; de Gouw, J. Observations of VOC Emissions and Photochemical Products over US Oil- and Gas-Producing Regions Using High-Resolution H_3O^+ CIMS (PTR-ToF-MS). *Atmospheric Meas. Technol.* **2017**, *10* (8), 2941−2968.
(20) Lerner, B. M.; Gilman, J. B.; Aikin, K. C.; Atlas, E. L.; Goldan, P. D.; Graus, M.; Hendershot, R.; Isaacman-VanWertz, G. A.; Koss, A.; Kuster, W. C.; Lueb, R. A.; McLaughlin, R. J.; Peischl, J.; Sueper, D.; Ryerson, T. B.; Tokarek, T. W.; Warneke, C.; Yuan, B.; de Gouw, J. A. An Improved, Automated Whole Air Sampler and Gas Chromatography Mass Spectrometry Analysis System for Volatile Organic Compounds in the Atmosphere. *Atmospheric Meas. Technol.* **2017**, *10* (1), 291−313.
(21) Veefkind, J. P.; Aben, I.; McMullan, K.; Förster, H.; de Vries, J.; Otter, G.; Claas, J.; Eskes, H. J.; de Haan, J. F.; Kleipool, Q.; van Weele, M.; Hasekamp, O.; Hoogeveen, R.; Landgraf, J.; Snel, R.; Tol, P.; Ingmann, P.; Voors, R.; Kruizinga, B.; Vink, R.; Visser, H.; Levelt, P. F. TROPOMI on the ESA Sentinel-5 Precursor: A GMES Mission for Global Observations of the Atmospheric Composition for Climate, Air Quality and Ozone Layer Applications. *Remote Sens. Environ.* **2012**, *120*, 70−83.
(22) van Geffen, J. H. G. M.; Boersma, K. F.; Van Roozendael, M.; Hendrick, F.; Mahieu, E.; De Smedt, I.; Sneep, M.; Veefkind, J. P. Improved Spectral Fitting of Nitrogen Dioxide from OMI in the 405—465 Nm Window. *Atmospheric Meas. Technol.* **2015**, *8* (4), 1685−1699.
(23) Vigouroux, C.; Langerock, B.; Bauer Aquino, C. A.; Blumenstock, T.; Cheng, Z.; De Mazière, M.; De Smedt, I.; Grutter, M.; Hannigan, J. W.; Jones, N.; Kivi, R.; Loyola, D.; Lutsch, E.; Mahieu, E.; Makarova, M.; Metzger, J.-M.; Morino, I.; Murata, I.; Nagahama, T.; Notholt, J.; Ortega, I.; Palm, M.; Pinardi, G.; Röhling, A.; Smale, D.; Stremme, W.; Strong, K.; Sussmann, R.; Té, Y.; van Roozendael, M.; Wang, P.; Winkler, H. TROPOMI—Sentinel-5 Precursor Formaldehyde Validation Using an Extensive Network of Ground-Based Fourier-Transform Infrared Stations. *Atmospheric Meas. Technol.* **2020**, *13* (7), 3751−3767.
(24) *S5P/TROPOMI HCHO ATBD*; S5P- BIRA-L2−400F- ATBD, 2022 (https://sentinels.copernicus.eu/documents/247904/2476257/Sentinel-5P-ATBD-HCHO-TROPOMI).
(25) van Geffen, J. H. G. M.; Eskes, H. J.; Boersma, K. F.; Veefkind, J. P.; *TROPOMI ATBD of the total and tropospheric NO2 data products*; S5P-KNMI-L2−0005-RP; 2022 (https://sentinels.copernicus.eu/documents/247904/2476257/Sentinel-5P-TROPOMI-ATBD-NO2-data-products).
(26) De Smedt, I.; Pinardi, G.; Vigouroux, C.; Compernolle, S.; Bais, A.; Benavent, N.; Boersma, F.; Chan, K.-L.; Donner, S.; Eichmann, K.-U.; Hedelt, P.; Hendrick, F.; Irie, H.; Kumar, V.; Lambert, J.-C.; Langerock, B.; Lerot, C.; Liu, C.; Loyola, D.; Piters, A.; Richter, A.; Rivera Cárdenas, C.; Romahn, F.; Ryan, R. G.; Sinha, V.; Theys, N.; Vlietinck, J.; Wagner, T.; Wang, T.; Yu, H.; Van Roozendael, M. Comparative Assessment of TROPOMI and OMI Formaldehyde Observations and Validation against MAX-DOAS Network Column Measurements. *Atmospheric Chem. Phys.* **2021**, *21* (16), 12561−12593.
(27) Gorchov Negron, A. M.; McDonald, B. C.; McKeen, S. A.; Peischl, J.; Ahmadov, R.; de Gouw, J. A.; Frost, G. J.; Hastings, M. G.; Pollack, I. B.; Ryerson, T. B.; Thompson, C.; Warneke, C.; Trainer, M. Development of a Fuel-Based Oil and Gas Inventory of Nitrogen Oxides Emissions. *Environ. Sci. Technol.* **2018**, *52* (17), 10175−10185.
(28) McDonald, B. C.; McBride, Z. C.; Martin, E. W.; Harley, R. A. High-Resolution Mapping of Motor Vehicle Carbon Dioxide Emissions. *J. Geophys. Res. Atmospheres* **2014**, *119* (9), 5283−5298.
(29) Pierce, T.Jr.; Geron, C.; Pouliot, G.; Kinnee, E.; Vukovich, J. Integration of the Biogenic Emissions Inventory System (BEIS3) into the Community Multiscale Air Quality Modeling System, In *18th International Emission Inventory Conference, Baltimore, Maryland*, 2009 vol. *14*, pp. 14-17.
(30) Coggon, M. M.; Gkatzelis, G. I.; McDonald, B. C.; Gilman, J. B.; Schwantes, R. H.; Abuhassan, N.; Aikin, K. C.; Arend, M. F.; Berkoff, T. A.; Brown, S. S.; Campos, T. L.; Dickerson, R. R.; Gronoff, G.; Hurley, J. F.; Isaacman-VanWertz, G.; Koss, A. R.; Li, M.; McKeen, S. A.; Moshary, F.; Peischl, J.; Pospisilova, V.; Ren, X.; Wilson, A.; Wu, Y.; Trainer, M.; Warneke, C. Volatile Chemical Product Emissions Enhance Ozone and Modulate Urban Chemistry. *Proc. Natl. Acad. Sci. U. S. A.* **2021**, *118* (32), No. e2026653118.
(31) Wolfe, G. M.; Marvin, M. R.; Roberts, S. J.; Travis, K. R.; Liao, J. The Framework for 0-D Atmospheric Modeling (F0AM) v3.1. *Geosci. Model Dev.* **2016**, *9* (9), 3309−3319.
(32) Jenkin, M. E.; Saunders, S. M.; Pilling, M. J. The Tropospheric Degradation of Volatile Organic Compounds: A Protocol for Mechanism Development. *Atmos. Environ.* **1997**, *31* (1), 81−104.
(33) Jenkin, M. E.; Saunders, S. M.; Wagner, V.; Pilling, M. J. Protocol for the Development of the Master Chemical Mechanism, MCM v3 (Part B): Tropospheric Degradation of Aromatic Volatile Organic Compounds. *Atmospheric Chem. Phys.* **2003**, 3 (1), 181−193.
(34) Saunders, S. M.; Jenkin, M. E.; Derwent, R. G.; Pilling, M. J. Protocol for the Development of the Master Chemical Mechanism, MCM v3 (Part A): Tropospheric Degradation of Non-Aromatic

https://doi.org/10.1021/acsearthspacechem.3c00203
ACS Earth Space Chem. XXXX, XXX, XXX−XXX

Volatile Organic Compounds. *Atmospheric Chem. Phys.* **2003**, *3* (1), 161−180.
(35) Jenkin, M. E.; Young, J. C.; Rickard, A. R. The MCM v3.3.1 Degradation Scheme for Isoprene. *Atmos. Chem. Phys.* **2015**, *15* (20), 11433−11459.
(36) Bloss, C.; Wagner, V.; Jenkin, M. E.; Volkamer, R.; Bloss, W. J.; Lee, J. D.; Heard, D. E.; Wirtz, K.; Martin-Reviejo, M.; Rea, G.; Wenger, J. C.; Pilling, M. J. Development of a Detailed Chemical Mechanism (MCMv3.1) for the Atmospheric Oxidation of Aromatic Hydrocarbons. *Atmos. Chem. Phys.* **2005**, *5* (3), 641−664.
(37) Goliff, W. S.; Stockwell, W. R.; Lawson, C. V. The Regional Atmospheric Chemistry Mechanism, Version 2. *Atmos. Environ.* **2013**, *68*, 174−185.
(38) Elvidge, C. D.; Zhizhin, M.; Baugh, K.; Hsu, F.-C.; Ghosh, T. Methods for Global Survey of Natural Gas Flaring from Visible Infrared Imaging Radiometer Suite Data. *Energies* **2016**, *9* (1), 14.
(39) Hersbach, H.; Bell, B.; Berrisford, P.; Hirahara, S.; Horányi, A.; Muñoz-Sabater, J.; Nicolas, J.; Peubey, C.; Radu, R.; Schepers, D.; Simmons, A.; Soci, C.; Abdalla, S.; Abellan, X.; Balsamo, G.; Bechtold, P.; Biavati, G.; Bidlot, J.; Bonavita, M.; De Chiara, G.; Dahlgren, P.; Dee, D.; Diamantakis, M.; Dragani, R.; Flemming, J.; Forbes, R.; Fuentes, M.; Geer, A.; Haimberger, L.; Healy, S.; Hogan, R. J.; Hólm, E.; Janisková, M.; Keeley, S.; Laloyaux, P.; Lopez, P.; Lupu, C.; Radnoti, G.; de Rosnay, P.; Rozum, I.; Vamborg, F.; Villaume, S.; Thépaut, J.-N. The ERA5 Global Reanalysis. *Q. J. R. Meteorol. Soc.* **2020**, *146* (730), 1999−2049.
(40) Majid, A.; Val Martin, M.; Lamsal, L. N.; Duncan, B. N. A Decade of Changes in Nitrogen Oxides over Regions of Oil and Natural Gas Activity in the United States. *Elem.: Sci. Anthropocene* **2017**, *5*, 76.
(41) Duncan, B. N.; Lamsal, L. N.; Thompson, A. M.; Yoshida, Y.; Lu, Z.; Streets, D. G.; Hurwitz, M. M.; Pickering, K. E. A Space-Based, High-Resolution View of Notable Changes in Urban NOx Pollution around the World (2005—2014). *J. Geophys. Res. Atmospheres* **2016**, *121* (2), 976−996.
(42) Dix, B.; de Bruin, J.; Roosenbrand, E.; Vlemmix, T.; Francoeur, C.; Gorchov-Negron, A.; McDonald, B.; Zhizhin, M.; Elvidge, C.; Veefkind, P.; Levelt, P.; de Gouw, J. Nitrogen Oxide Emissions from U.S. Oil and Gas Production: Recent Trends and Source Attribution. *Geophys. Res. Lett.* **2020**, *47* (1), e2019GL085866.
(43) de Gouw, J. A.; Veefkind, J. P.; Roosenbrand, E.; Dix, B.; Lin, J. C.; Landgraf, J.; Levelt, P. F. Daily Satellite Observations of Methane from Oil and Gas Production Regions in the United States. *Sci. Rep.* **2020**, *10* (1), 1379.
(44) McDuffie, E. E.; Edwards, P. M.; Gilman, J. B.; Lerner, B. M.; Dubé, W. P.; Trainer, M.; Wolfe, D. E.; Angevine, W. M.; deGouw, J.; Williams, E. J.; Tevlin, A. G.; Murphy, J. G.; Fischer, E. V.; McKeen, S.; Ryerson, T. B.; Peischl, J.; Holloway, J. S.; Aikin, K.; Langford, A. O.; Senff, C. J.; Alvarez, R. J., II; Hall, S. R.; Ullmann, K.; Lantz, K. O.; Brown, S. S. Influence of Oil and Gas Emissions on Summertime Ozone in the Colorado Northern Front Range. *J. Geophys. Res. Atmospheres* **2016**, *121* (14), 8712−8729.
(45) Green, J. R.; Fiddler, M. N.; Fibiger, D. L.; McDuffie, E. E.; Aquino, J.; Campos, T.; Shah, V.; Jaeglé, L.; Thornton, J. A.; DiGangi, J. P.; Wolfe, G. M.; Bililign, S.; Brown, S. S. Wintertime Formaldehyde: Airborne Observations and Source Apportionment Over the Eastern United States. *J. Geophys. Res. Atmospheres* **2021**, *126* (5), No. e2020JD033518.
(46) Pikelnaya, O.; Flynn, J. H.; Tsai, C.; Stutz, J. Imaging DOAS Detection of Primary Formaldehyde and Sulfur Dioxide Emissions from Petrochemical Flares. *J. Geophys. Res. Atmospheres* **2013**, *118* (15), 8716−8728.
(47) Luecken, D. J.; Hutzell, W. T.; Strum, M. L.; Pouliot, G. A. Regional Sources of Atmospheric Formaldehyde and Acetaldehyde, and Implications for Atmospheric Modeling. *Atmos. Environ.* **2012**, *47*, 477−490.
(48) Zhu, L.; Jacob, D. J.; Keutsch, F. N.; Mickley, L. J.; Scheffe, R.; Strum, M.; González Abad, G.; Chance, K.; Yang, K.; Rappenglück, B.; Millet, D. B.; Baasandorj, M.; Jaeglé, L.; Shah, V. Formaldehyde (HCHO) As a Hazardous Air Pollutant: Mapping Surface Air Concentrations from Satellite and Inferring Cancer Risks in the United States. *Environ. Sci. Technol.* **2017**, *51* (10), 5650−5657.
(49) Lerot, C.; Hendrick, F.; Van Roozendael, M.; Alvarado, L. M. A.; Richter, A.; De Smedt, I.; Theys, N.; Vlietinck, J.; Yu, H.; Van Gent, J.; Stavrakou, T.; Müller, J.-F.; Valks, P.; Loyola, D.; Irie, H.; Kumar, V.; Wagner, T.; Schreier, S. F.; Sinha, V.; Wang, T.; Wang, P.; Retscher, C. Glyoxal Tropospheric Column Retrievals from TROPOMI — Multi-Satellite Intercomparison and Ground-Based Validation. *Atmospheric Meas. Technol.* **2021**, *14* (12), 7775−7807.

https://doi.org/10.1021/acsearthspacechem.3c00203
ACS Earth Space Chem. XXXX, XXX, XXX−XXX